Hybrid Position Sensorless Vector Control of a Reluctance Synchronous Machine through the Entire Speed Range

W.T. Villet*, M.J. Kamper*, P. Landsmann† and R. Kennel†

* Stellenbosch University, Stellenbosch, 15053830@sun.ac.za, kamper@sun.ac.za
†Technische Universitaet Munich, Munich, Germany, peter.landsmann@tum.de,ralph.kennel@tum.de

***Abstract*—In this paper a new hybrid position sensorless control scheme for reluctance synchronous machine drives is introduced. The scheme combines a simplified alternating high frequency injection position sensorless control method with a relatively new fundamental saliency based position sensorless control method. Separate phase locked loops and current controllers are designed and implemented for each method, thus ensuring optimum performance of each method. The synchronisation of the two phase locked loops, combined with a hysteresis changeover threshold, ensures seamless transition between the two estimation methods. Current- and speed control is shown to be possible through the entire speed range at high loads.**

***Index Terms*—Hybrid sensorless control, Reluctance synchronous machines, Variable speed drives**

NOMENCLATURE AND DEFINITIONS

Symbols:

u, i, ψ	Voltage current and flux linkage
R, L	Resistance and inductance
Y	Admittance
T_M, Θ	Mechanical torque and inertia
θ_r, ω_r	Rotor- angle and speed
θ_e, ω_e	Electrical- rotor angle and speed
Δ, Σ	Difference and sum

Indices:

s, r	Stator and rotor
a, b, c	Stator phase axes
α, β	Stator fixed cartesian axes
d, q	Rotor fixed direct and quadrature axes
c	Carrier frequency

Scalar values are written in normal letters, e.g. R or τ, vector values are written in small bold letters, e.g. $\mathbf{i}$ or $\boldsymbol{\psi}$, and tensor matrices are written in bold capital letters, e.g. $\mathbf{L}$ or $\mathbf{T}$. Subscripts describe the location of the physical quantity, e.g. R_s is the stator resistance. Superscripts specify the reference frame of the quantity, e.g. $\mathbf{i}_s^{(r)}$ is the stator current vector in the rotor reference frame. Superscript ^{T} is used to transpose a vector and superscript $^{-1}$ for the inverse.

Vectors are transposed from one reference frame to another with $\mathbf{T}(r \rightarrow s)$ or $\mathbf{T}(s \rightarrow r)$.

$$\mathbf{T} = \begin{bmatrix} cos(\theta_e) & -sin(\theta_e) \\ sin(\theta_e) & cos(\theta_e) \end{bmatrix}$$

$$\mathbf{T}^{-1} = \begin{bmatrix} cos(\theta_e) & sin(\theta_e) \\ -sin(\theta_e) & cos(\theta_e) \end{bmatrix}$$

The matrix $\mathbf{J}$ is used for orthogonal rotation, that is

$$\mathbf{J} \quad = \quad \mathbf{T}(\frac{\pi}{2}) = \begin{bmatrix} 0 & -1 \\ 1 & 0 \end{bmatrix}.$$

$\mathbf{T}$ and $\mathbf{J}$ are the vector equivalents of the complex operators $e^{j\theta}$ and j respectively. Derivatives with respect to time are indicated by a dot, e.g $\dot{\mathbf{i}}_s^{(r)}$, and derivatives with respect to rotor angle with an prime, e.g. $\mathbf{L}_s^{(s)'}$. Estimated quantities are indicted with a hat, e.g. $\hat{\theta}_e$.

I. INTRODUCTION

The reluctance synchronous machine (RSM) is known to be robust and comparably efficient under field oriented control algorithms [1] [2]. These advantages, among others, has led to a new-found interest in these AC machines that do not have rotor windings or permanent magnets. A position sensor is necessary to obtain the rotor position to implement field oriented control. Position sensors, however, are expensive, take up space and are not suitable for harsh environments.

Various methods of position sensorless control have been developed over the years. Back EMF position sensorless methods are used with permanent magnet machines to detect the rotor position at medium to high speeds [3]. This method of position detection is not possible for the RSM due to the only source of flux being the stator currents. In [4], a fundamental saliency based tracking scheme is proposed for the RSM. This method takes into account the non-linear relationship between the isotropic flux and current, and makes it possible to produce high torque with good dynamics. Rotor position estimation is not possible at low speeds and standstill with the fundamental saliency method, as with the back EMF methods.

Several authors have investigated different variations of hybrid methods for permanent magnet machines to overcome the shortcoming of the back EMF method at standstill and to implement control through the entire speed range of the drive [5]–[8].

A high frequency assisted active flux based sensorless method for axially laminated anisotropic (ALA) RSM's is proposed in [9]. In this method the difference between the two estimated angles of the two position estimation methods are fed through a PI controller which gradually changes gain at high speeds allowing only the active flux method to do position estimation at high speeds.

A current-frequency method with coupled active flux based sensorless control for RSM's is proposed in [10]. This method performs open loop control at standstill and low speeds. In [11] a method is proposed for the RSM that utilises the indirect flux detection by an on-line reactance measurement (INFORM) model at low speeds and an EMF model at high speeds. A hybrid method combining high frequency injection with flux estimation is proposed for the RSM in [12]. This method is supported by a speed observer. Changeover from one scheme to another is done gradually with speed dependent gains. Due to the nature of the changeover between the two schemes both estimation schemes are driven by the same current controller gains.

The method proposed in this paper utilises the non-linear fundamental saliency estimation method (FSM) proposed by [4], combined with a simplified alternating high frequency carrier injection method [13]. The proposed scheme has the aim to utilize optimum performance of each scheme by implementing unique current controller- and phase locked loop (PLL) gains for each method.

II. Basic RSM Operation

The RSM investigated is as shown in Fig. 1. This RSM is a transverse laminated 2-pole pair motor with distributed stator windings. The rotor has two flux barriers. The q-axis is algined along the minimum permeance axes in quadrature with the flux barriers. The d-axis is aligned with the maximum permeance axis, along the rotor iron segments. This difference in permeance creates the RSM's high saliency. It is shown later in this paper that no or little inductance saliency exists at small current magnitudes. A small current is always applied to the q-axis to saturate the q-axis magnetic circuit, thus ensuring a large enough saliency.

It is shown in [14] that the maximum torque per ampere locus of the RSM can be approximated by a current angle of 60^o. The current vector at low loads ensures an always present q-axis current for visible saliency, but approaches a current angle of 60^o as the load increases, ensuring maximum torque per ampere.

The only source of flux is the stator coils. Hence the RSM is described electrically by the stator voltage equation of (1). The vector product of the flux and the current gives the torque of the machine as given by (2).

$$\mathbf{u}_S^{(s)} = R_s \mathbf{i}_s^{(s)} + \dot{\boldsymbol{\psi}}_s^{(s)} \tag{1}$$

$$T_m = \frac{3p}{2} {\mathbf{i}_s^{(r)}}^T \mathbf{J} \boldsymbol{\psi}_{\boldsymbol{s}}^{(\boldsymbol{r})} = \frac{3p}{2}(\psi_d i_q - \psi_q i_d) \tag{2}$$

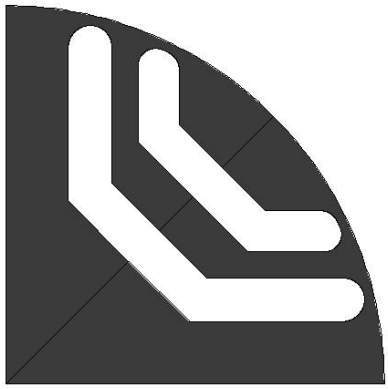

Fig. 1. Geometery of the investigated RSM.

III. Alternating High Frequency Injection Method

In this method a high frequency (HF) voltage vector is superimposed onto the fundamental control voltage vector in the estimated rotary reference frame. An amplitude modulation scheme is used to track the saliency induced by the saturation along the axis orthogonal to the injection axis [15]. With proper demodulation it is possible to track the anisotropy position [16]. The anisotropy in a reluctance synchronous machine rotates at the same angular frequency as the rotor.

At high frequencies, that are bounded by (3) where f_s is the sampling frequency, the RSM can be described as in (4), consisting out of only an inductance voltage term [15] [17].

$$2\omega_r < \omega_{HF} < \frac{2\pi f_s - 2\omega_r}{2} \tag{3}$$

$$\mathbf{u}_{sc}^{(r)} = \mathbf{L}^{(r)} \frac{d\mathbf{i}_{sc}^{(r)}}{dt} \tag{4}$$

$\mathbf{L}^{(r)}$ is the tangential inductance matrix defined as in (5) [17]. The injected carrier voltage is defined as in (6), where ω_c is the constant carrier frequency (injection frequency). The high frequency carrier injection occurs on the estimated d-axis with the estimated electrical angle, $\hat{\theta}_e$.

$$\mathbf{L}^{(r)} = \begin{bmatrix} L_d & 0 \\ 0 & L_q \end{bmatrix} \tag{5}$$

$$\mathbf{u}_{sc}^{(\hat{r})} = \begin{bmatrix} u_c cos(\omega_c t) \\ 0 \end{bmatrix} \tag{6}$$

Equations (4) and (6) can be used to describe the high frequency measured current as in (7) [17] [18].

$$\begin{aligned} \mathbf{i}_{sc}^{(\hat{r})} &= {\mathbf{L}^{(\hat{r})}}^{-1} \int \mathbf{u}_{sc}^{(\hat{r})} dt \\ &= \frac{u_c sin(\omega_c t)}{L_d L_q \omega_c} \left(L_\Sigma \begin{bmatrix} 1 \\ 0 \end{bmatrix} - \Delta L \begin{bmatrix} cos(2\Delta\theta_e) \\ sin(2\Delta\theta_e) \end{bmatrix} \right) \end{aligned} \tag{7}$$

In (7), $L_\Sigma = (L_d + L_q)/2$ is the mean position independent inductance and $\Delta L = (L_d - L_q)/2$ is the

inductance saliency. The estimation error is defined as $\Delta\theta_e = \theta_e - \hat{\theta}_e$. Conventional HF methods filter i_q with a band-pass filter to extract the frequency component that has information regarding the position estimation error before frequency shifting the HF components back to the origin.

It is shown in [13] that the component that contains information regarding the position estimation error is separated from the other high frequency components by twice the carrier frequency if the band-pass filter is omitted in the demodulation scheme. This concept simplifies the demodulation scheme by directly frequency shifting the q-axis current whereafter it is low-pass filtered to reject the high frequency components. Using fewer filters increases the dynamic performance and reduces phase lag and time delay. Finally the demodulated q-axis current is used to drive a phase locked loop (PLL) to extract the estimated electrical angle, $\hat{\theta}_e$ [16], [17]. The PLL is implemented with a simple PI controller.

The simplified high frequency injection method as implemented in this project is illustrated in Fig. 2. An important aspect to note about this method is that the position estimation error that is driven through a PLL is scaled by the magnitude of the inductance saliency ΔL. This implies that this method is dependent on a large enough inductance saliency.

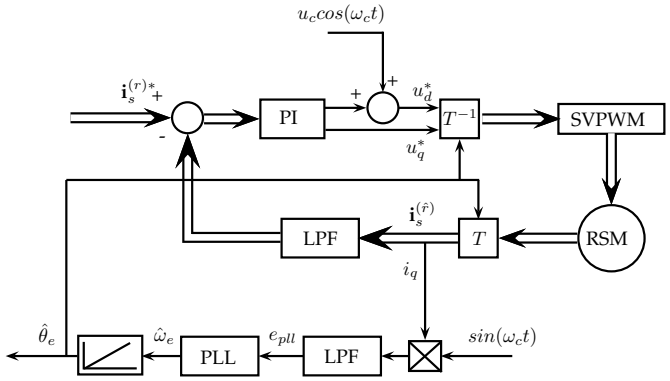

Fig. 2. Block diagram of simplified alternating high frequency injection position sensorless control.

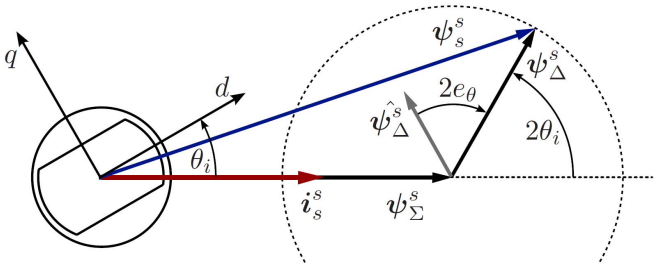

Fig. 3. Flux linkage orientation due to saliency [4].

IV. Fundamental Saliency Based Estimation Method

If it is assumed that the flux linkage vector is linearly dependent on the current vector, the flux linkage vector can be calculated with the secant (instantaneous) inductance defined as in (8). With this assumption it is now possible to describe the stator flux vector in the stationary reference frame with (9) [4] where L_Δ is the secant (instantaneous) inductance saliency and equals $(L_d - L_q)/2$.

$$\mathbf{L} = \frac{\boldsymbol{\psi}_s^{(r)}}{\mathbf{i}_s^{(s)}} \tag{8}$$

$$\begin{aligned} \boldsymbol{\psi}_s^{(s)} &= L_\Sigma \mathbf{i}_s^{(s)} + L_\Delta \begin{bmatrix} cos(2\theta_e) & sin(2\theta_e) \\ sin(2\theta_e) & -cos(2\theta_e) \end{bmatrix} \mathbf{i}_s^{(s)} \\ &= \boldsymbol{\psi}_\Sigma^{(s)} + \boldsymbol{\psi}_\Delta^{(s)} \end{aligned} \tag{9}$$

As shown in Fig. 3, [4] stated that $\boldsymbol{\psi}_\Sigma^{(s)}$ is parallel to the current vector and that the fundamental saliency, $\boldsymbol{\psi}_\Delta^{(s)}$, rotates with double the rotor speed while having a constant magnitude. θ_i is defined by [4] as the angle between the current and the rotor d-axis. When rearranging (9) and (10), it is possible to calculate the fundamental saliency, $\boldsymbol{\psi}_\Delta^s$ with measurable quantities as in (11). The relationship between current and flux is not linear as expected, thus $\boldsymbol{\psi}_\Sigma^{(s)}$ can not be calculated directly. Instead, lookup tables can be used as shown in (12) [4].

$$\mathbf{u}_s^{(s)} = R_s \mathbf{i}_s^{(s)} + \dot{\boldsymbol{\psi}}_s^{(s)} \tag{10}$$

$$\begin{aligned} \boldsymbol{\psi}_\Delta^{(s)} &= \boldsymbol{\psi}_s^{(s)} - \boldsymbol{\psi}_\Sigma^{(s)} \\ &= \int \mathbf{u}_s^{(s)} - R_s \mathbf{i}_s^{(s)} dt - \boldsymbol{\psi}_\Sigma^{(s)}(\mathbf{i}_s^s) \end{aligned} \tag{11}$$

$$\begin{aligned} \boldsymbol{\psi}_\Sigma^{(s)}(\mathbf{i}_s^s) &= \frac{\psi_d(|\mathbf{i}_s^s|, 0) + \psi_q(0, |\mathbf{i}_s^s|)}{2} \frac{\mathbf{i}_s^s}{|\mathbf{i}_s^s|} \\ &= \psi_\Sigma(|\mathbf{i}_s^s|) \frac{\mathbf{i}_s^s}{|\mathbf{i}_s^s|} \end{aligned} \tag{12}$$

It is also possible to calculate $\boldsymbol{\psi}_\Delta^{(s)}$ in the estimated reference frame with (13), by using the estimated electrical position, $\hat{\theta}_e$, which is tracked by the PLL. An angle difference between the two vectors, $\boldsymbol{\psi}_\Delta^{(s)}$ and $\hat{\boldsymbol{\psi}}_\Delta^{(s)}$ can be calculated by taking the vector product as in (14) [4]. This angle is equal to the position estimation error and can be fed back to the PLL, which is a PI controller that will drive the error to zero [4].

$$\hat{\boldsymbol{\psi}}_\Delta^{(s)} = L_\Delta \begin{bmatrix} cos(2\hat{\theta}_e) & sin(2\hat{\theta}_e) \\ sin(2\hat{\theta}_e) & -cos(2\hat{\theta}_e) \end{bmatrix} \mathbf{i}_s^{(s)} \tag{13}$$

$$\begin{aligned} \Delta\theta_e &= {\boldsymbol{\psi}_\Delta^{(s)}}^T \mathbf{J} \hat{\boldsymbol{\psi}}_\Delta^{(s)} \\ &= |\boldsymbol{\psi}_\Delta^{(s)}||\hat{\boldsymbol{\psi}}_\Delta^{(s)}| sin(2\Delta\theta_e) \end{aligned} \tag{14}$$

During voltage integration in (11), integrator drift can occur. Integration drift can be compensated for by subtracting $k_d \boldsymbol{\psi}_\Delta^{(s)}$ within the integration of (11) [4], i.e.

$$\boldsymbol{\psi}_\Delta^{(s)} = \int \mathbf{u}_s^{(s)} - R_s \mathbf{i}_s^{(s)} - k_d \boldsymbol{\psi}_\Delta^{(s)} dt - L_\Sigma \mathbf{i}_s^{(s)}. \tag{15}$$

The non-linear fundamental saliency position sensorless control method (FSM) as implemented is illustrated in Fig. 4.

V. Hybrid Estimation Scheme

Both the discussed methods have their advantages and drawbacks. The HF injection method has the advantage that it can detect the rotor position at standstill and at very low speeds. The drawback is that the injected voltage takes up a large portion of the DC bus voltage, limiting the voltage that can be supplied by the inverter to implement control. HF signals can also cause torque ripple and can have negative effects on the control structure. As stated earlier this method also relies on a strong enough inductance saliency ΔL. This inductance saliency tends to disappear under very low- and very high loads.

The FSM make use of the full DC link bus voltage. This allows this method to achieve rated torque at rated speed under speed and current control. This method is also more dynamic than the HF method at high speeds. The FSM relies on the fundamental saliency for position estimation. Unlike the inductance saliency that is required for the HF method, the fundamental saliency does not disappear at high loads, making the FSM method effective under high load conditions. Due to parameter errors and drift effects, the scheme is unstable at very low speeds and standstill. Combining the two schemes, will utilise the advantages of both schemes while eliminating some drawbacks like the lack of position estimation at standstill, acoustic noise at high speeds and limited torque capabilities.

A. Changeover

The changeover between the estimation methods needs to be seamless and effective. The changeover used in this project is based on a hysteresis effect. During acceleration from standstill a changeover from the HF method to the FSM method is chosen at a speed of 0.43 $p.u$ (65 rad/s). During deceleration the changeover from the FSM method to HF method is chosen at a speed of 0.26 $p.u$. (40 rad/s). Using two different speed points for changeover instead of one single speed threshold, has the drawback that during acceleration the changeover is slightly higher than it needs to be (0.43 $p.u$ instead of 0.26 $p.u$). It does however have the advantage that a speed ripple around the changeover thresholds won't result in an unnecessary back and forth switching between estimation methods.

Due to the difference in the two schemes it was found that they react differently to control- and PLL gains. With the hysteresis changeover scheme it is possible to drive each scheme with its own optimised current controller and PLL gains, ensuring optimum performance from each scheme.

The main contribution of this work is the PLL synchronisation. To ensure seamless changeover between the position estimation methods, the two PLL's of the two methods are synchronised by feeding the estimated angle and speed from the active PLL to the inactive one right before changeover. This allows the PLL to directly track the angle at changeover. In the implementation of the scheme the FSM is always active, although not always in control, but the HF injection scheme is switched off when not in use, thus freeing up the DC bus. The working of the changeover and PLL synchronosation is shown in Fig. 5.

VI. Measured Results

The specifications of the RSM used are listed in Table I. The RSM is coupled to an induction machine (IM) as load. Each machine is driven by a 5 kW inverter with the DC links bridged. The inverters are controlled by a LINUX based real time application interface.

TABLE I
RSM specifications

Pole pairs	2	
Nominal power	1.1	kW
Rated current	3.5	A RMS
Rated mechanical torque	7	Nm
Rated mechanical speed	157	rad/s

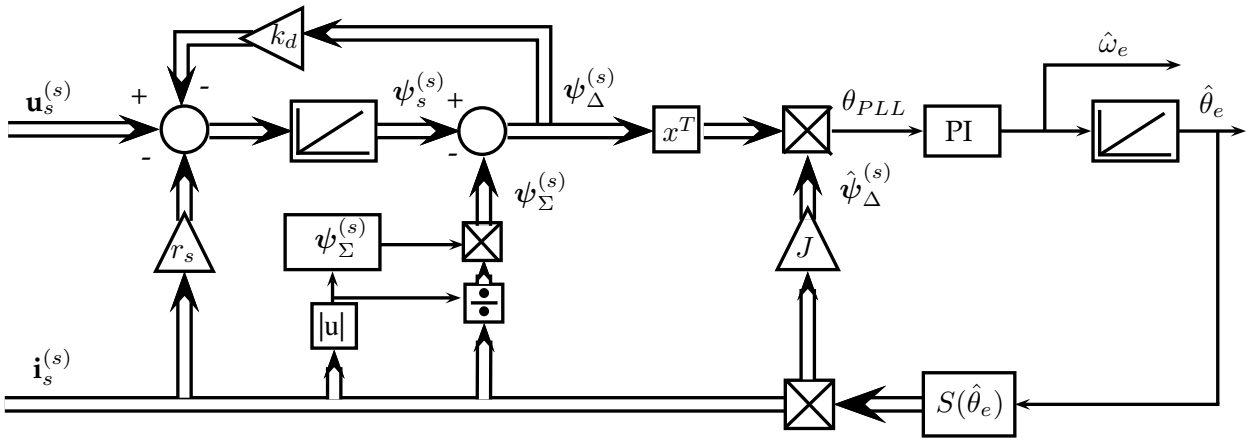

Fig. 4. Non-linear funamental saliency position estimation scheme.

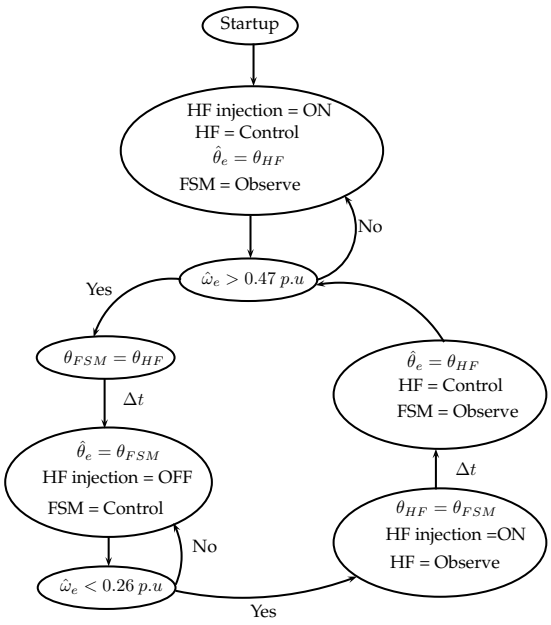

Fig. 5. State space diagram of the hybrid position sensorless control method.

The test bench used is shown in Fig. 6. The blue machine is the IM and the orange the RSM. The measured uncoupled flux linkage and inductance curves of the RSM are displayed in Fig. 7 as a function of current. The second frame shows how the inductance saliency ΔL disappears at high currents.

A. Limits of Stable Operation

The limits of stable stationary operation indicate what torque the hybrid method is able to deliver as a function of speed. The resultant stable area of operation is shown in Fig. 8. The hysteresis effect is clearly visible in the middle of Fig. 8 due to the two changeover threshold values. The upper part of the hysteresis is the FSM and the lower part is the HF injection method.

Saturation of the flux linkage at low speed under high load causes the HF method to lose track due to a disappearing inductance saliency, as seen in Fig. 7. Although

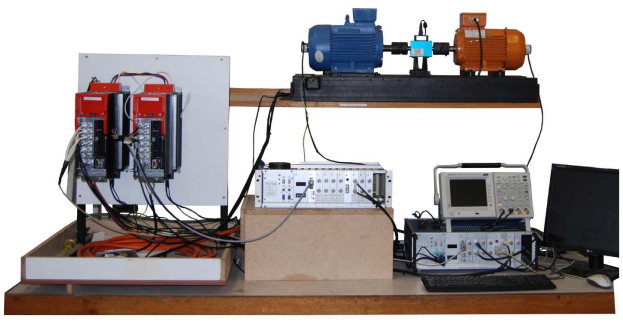

Fig. 6. Test bench used with the IM on the left and the RSM on the right.

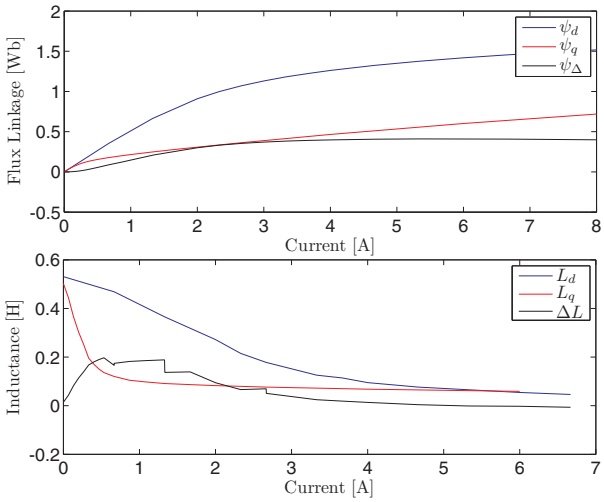

Fig. 7. Measured flux linkage and inductance curves as a function of current.

limited by the HF method, the startup torque with current control is almost double the rated torque, thus overcoming the problems perceived by [6]. The results in Fig. 8 show that despite very high loads, the proposed scheme is able to track the rotor position in the entire speed region of the drive and is only limited by the DC bus voltage at medium to high speeds.

B. Speed Response

The speed response of the hybrid scheme includes the investigation of the changeover between the two methods. A speed step of $1.33\ p.u$ is applied to the RSM-drive at standstill as shown in Fig. 9. It is clear that the changeover is seamless, even when a speed step of above rated speed is applied and removed.

C. Load tests

In Fig. 10 the position sensorless controlled RSM is in speed control. With the reference speed set to $0\ p.u$ a load

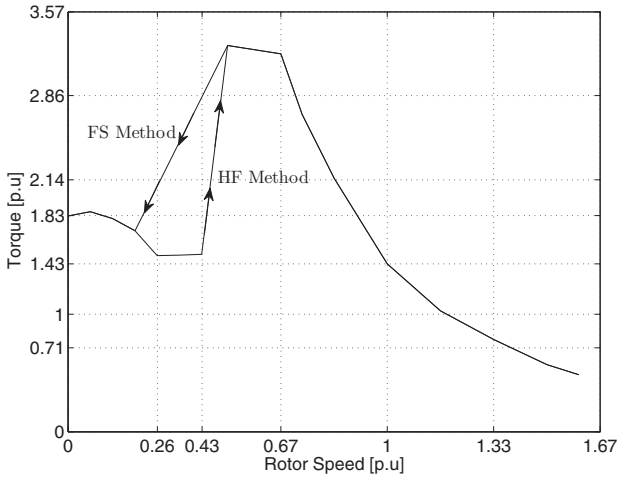

Fig. 8. Limits of stable operation of the RSM under current control.

of rated torque is applied to the RSM. The second frame shows that the steady state position estimation error does not exceed $|5^o|$ electrical.

In Fig. 11 the position sensorless controlled RSM speeds up to rated speed from standstill. Full load is applied and removed to the RSM at rated speed. The speed then changes to a negative direction where torque is again applied and removed to the RSM, this time in the opposite direction. These tests display the hybrid method's ability to respond to speed steps, change in speed direction and applied load. The position estimation error in Fig. 11 never exceeds $|15^o|$, while its steady state value is below $|10^o|$.

D. Hysteresis Analysis

The purpose of having a hysteresis changeover is to avoid unnecessary switching between the schemes during a speed ripple. To investigate the feasibility of this argument the RSM speeds up to activate the FSM and is then lowered to the middle of the hysteresis region ensuring that the fundamental method is still active. A series of tests are performed in this region.

Figure 12 shows the results of a large torque step in this region. The first screen shows the torque step and the second screen indicates which estimation scheme is active. As the speed drops, one changeover occurs due to undershoot, and during the removal of the step another changeover occurs during overshoot. It is clear that there is no unnecessary back and forth switching between the estimation schemes.

The effect of variable torque switching on the scheme is investigated in Fig. 13. While operating in the middle of the hysteresis region the load is applied and removed several times with impulse like characteristics. Again, it is clear that there is no unnecessary back and forth switching between the two schemes except when the load causes under- or overshoot.

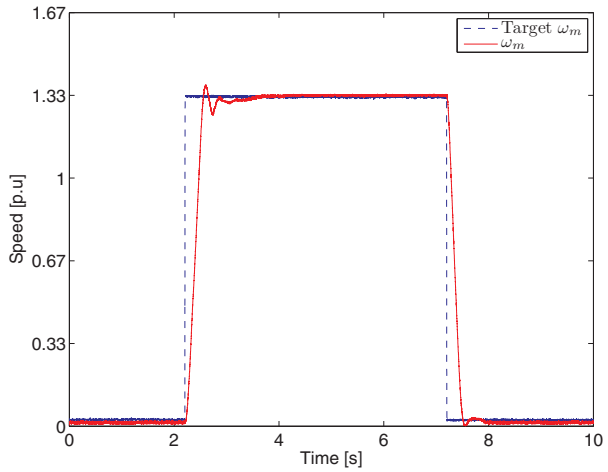

Fig. 9. No load RSM speed response.

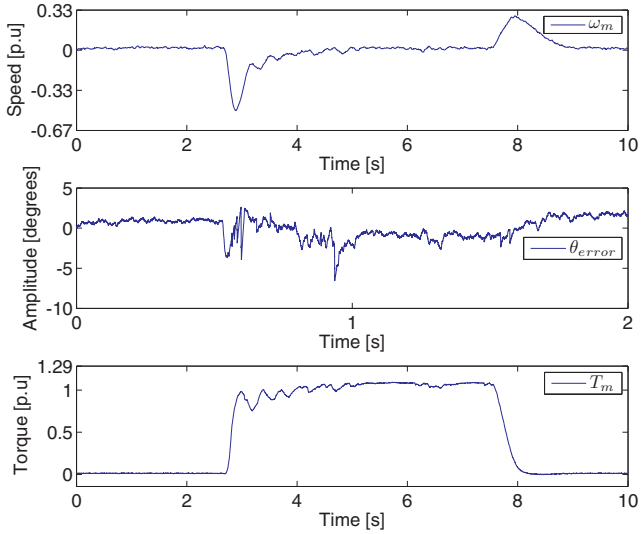

Fig. 10. Zero speed operation in speed control while applying rated torque to RSM.

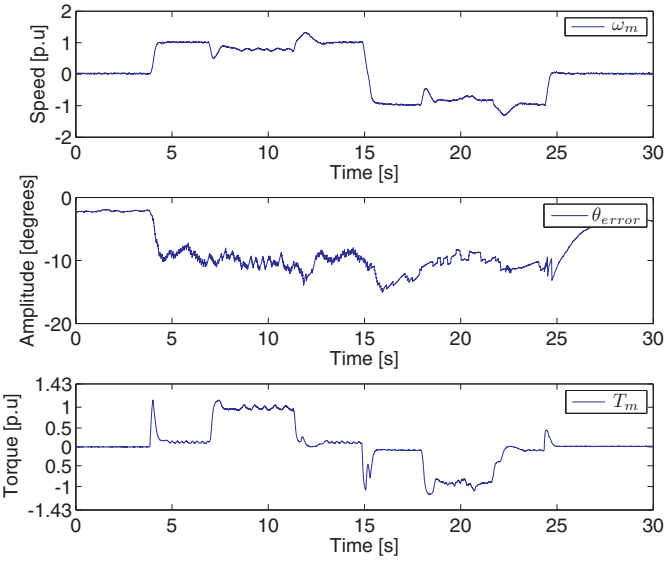

Fig. 11. From zero to speeds of 1 $p.u$ and -1 $p.u$ with torque perturbations.

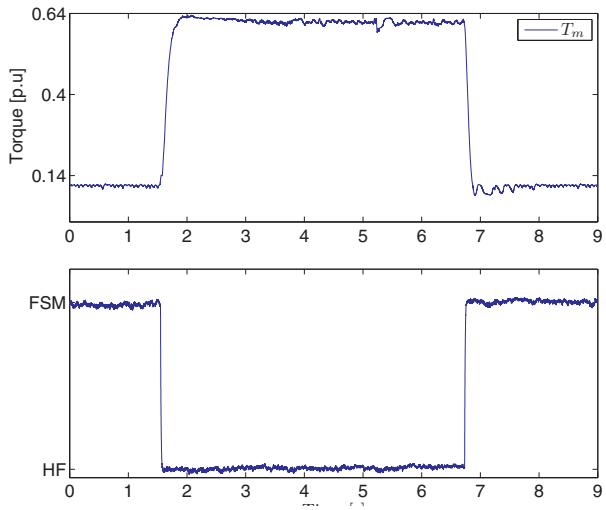

Fig. 12. Hybrid method response to large applied load in the middle of the hysteresis region.

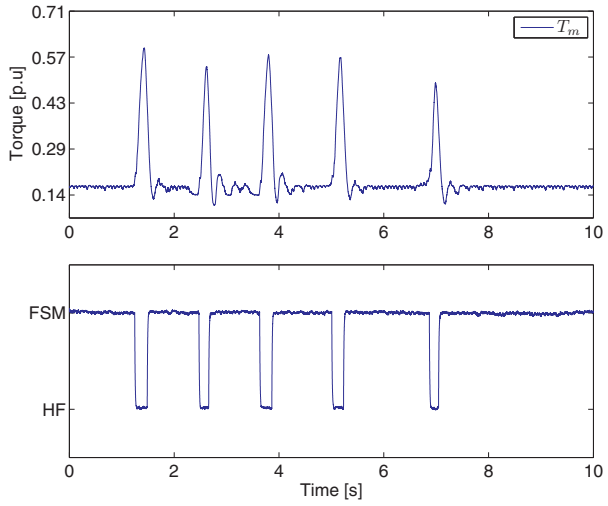

Fig. 13. Hybrid method response to impulses of large applied load in the middle of the hysteresis region.

VII. Conclusion

A hybrid position estimation scheme that makes use of a simplified alternating high frequency injection- and a fundamental saliency based position sensorless control methods, is introduced in this paper. Seamless changeover between the two estimation methods is achieved by synchronising the two PLL's when changing between estimation methods, while implementing each method with optimum performance driven gains. A hysteresis based changeover is proposed to prevent back and forth switching between the two estimation methods. Measured results show that the implementation of hysteresis changeover is successful and no unnecessary switching between the two methods occurs. Even under impulse-like load addition and removals, the method is stable.

It can be concluded from measured results that the implementation of the method is successful and that the hybrid method is able to produce high torque from startup up to base speed, overcoming problems perceived by [6]. Tests show that there are no noticeable effects in machine response when changeover occurs, thus providing evidence of a successful changeover method. Furthermore, measured results show that the hybrid method is able to change direction from positive rated speed to negative rated speed. The ability to accurately estimate the rotor position during direction change improves on previous work done by [10].

References

[1] A. Fratta and A. Vagati, "A reluctance motor drive for high dynamic performance application," *IEEE Transactions on Industry Applications*, vol. 28, no. 4, pp. 873 –879, jul/aug 1992.

[2] R. Trubenbach, A. Mackay, and M. Kamper, "Performance of a reluctance synchronous machine under vector control," in *Power Electronics Specialists Conference, 1993. PESC '93 Record., 24th Annual IEEE*, jun 1993, pp. 803 –808.

[3] F. Genduso, R. Miceli, C. Rando, and G. Galluzzo, "Back emf sensorless-control algorithm for high-dynamic performance pmsm," *Industrial Electronics, IEEE Transactions on*, vol. 57, no. 6, pp. 2092 –2100, june 2010.

[4] P. Landsmann, R. Kennel, H. de Kock, and M. Kamper, "Fundamental saliency based encoderless control for reluctance synchronous machines," in *Electrical Machines (ICEM), 2010 XIX International Conference on*, sept. 2010, pp. 1 –7.

[5] K. Ide, H. Iura, and M. Inazumi, "Hybrid sensorless control of ipmsm combining high frequency injection method and back emf method," in *IECON 2010 - 36th Annual Conference on IEEE Industrial Electronics Society*, nov. 2010, pp. 2236 –2241.

[6] Y. Yamamoto, H. Funato, and S. Ogasawara, "Hybrid sensor-less control of permanent magnet synchronous motor in low-speed region," in *Power Electronics, 2007. ICPE '07. 7th Internatonal Conference on*, oct. 2007, pp. 823 –828.

[7] C. Silva, G. Asher, and M. Sumner, "Hybrid rotor position observer for wide speed-range sensorless pm motor drives including zero speed," *Industrial Electronics, IEEE Transactions on*, vol. 53, no. 2, pp. 373 – 378, april 2006.

[8] J.-H. Lee, T.-W. Kong, W.-C. Lee, C.-Y. Won, and J.-S. Yu, "A new hybrid sensorless method using a back emf estimator and a current model of permanent magnet synchronous motor," in *Power Electronics Specialists Conference, 2008. PESC 2008. IEEE*, june 2008, pp. 4256 –4262.

[9] S.-C. Agarlita, I. Boldea, and F. Blaabjerg, "High frequency injection assisted "active flux" based sensorless vector control of reluctance synchronous motors, with experiments from zero speed," in *Energy Conversion Congress and Exposition (ECCE), 2011 IEEE*, sept. 2011, pp. 2725 –2732.

[10] S.-C. Agarlita, M. Fatu, L. Tutelea, F. Blaabjerg, and I. Boldea, "I-f starting and active flux based sensorless vector control of reluctance synchronous motors, with experiments," in *Optimization of Electrical and Electronic Equipment (OPTIM), 2010 12th International Conference on*, may 2010, pp. 337 –342.

[11] M. Schroedl and P. Weinmeier, "Sensorless control of reluctance machines at arbitrary operating conditions including standstill," *Power Electronics, IEEE Transactions on*, vol. 9, no. 2, pp. 225 –231, mar 1994.

[12] J.-I. Ha, S.-J. Kang, and S.-K. Sul, "Position-controlled synchronous reluctance motor without rotational transducer," *Industry Applications, IEEE Transactions on*, vol. 35, no. 6, pp. 1393 –1398, nov/dec 1999.

[13] W. Villet and M. Kamper, "Evaluation of a simplified HF injection position sensorless control method for reluctance synchronous machine drives," in *Power Electronics and Machine Drives Conference (PEMD) Bristol, UK*, March 2012.

[14] H. De Kock, M. Kamper, and R. Kennel, "Anisotropy comparison of reluctance and pm synchronous machines for position sensorless control using hf carrier injection," *Power Electronics, IEEE Transactions on*, vol. 24, no. 8, pp. 1905 –1913, aug. 2009.

[15] D. Raca, P. Garcia, D. Reigosa, F. Briz, and R. Lorenz, "A comparative analysis of pulsating vs. rotating vector carrier signal injection-based sensorless control," in *Applied Power Electronics Conference and Exposition, 2008. APEC 2008. Twenty-Third Annual IEEE*, feb. 2008, pp. 879 –885.

[16] M. Linke, R. Kennel, and J. Holtz, "Sensorless speed and position control of synchronous machines using alternating carrier injection," in *Electric Machines and Drives Conference, 2003. IEMDC'03. IEEE International*, vol. 2, June 2003, pp. 1211 – 1217 vol.2.

[17] W. Hammel and R. Kennel, "Position sensorless control of PMSM by synchronous injection and demodulation of alternating carrier voltage," in *Sensorless Control for Electrical Drives (SLED), 2010 First Symposium on*, july 2010, pp. 56 –63.

[18] R. Leidhold and P. Mutschler, "Improved method for higher dynamics in sensorless position detection," in *Industrial Electronics, 2008. IECON 2008. 34th Annual Conference of IEEE*, nov. 2008, pp. 1240 –1245.